Pattern Analysis of Dynamic Susceptibility Contrast-enhanced MR Imaging Demonstrates Peritumoral Tissue Heterogeneity[1]

Hamed Akbari, MD, PhD
Luke Macyszyn, MD, MA
Xiao Da, MS
Ronald L. Wolf, MD, PhD
Michel Bilello, MD, PhD
Ragini Verma, PhD
Donald M. O'Rourke, MD
Christos Davatzikos, PhD

Purpose: To augment the analysis of dynamic susceptibility contrast material–enhanced magnetic resonance (MR) images to uncover unique tissue characteristics that could potentially facilitate treatment planning through a better understanding of the peritumoral region in patients with glioblastoma.

Materials and Methods: Institutional review board approval was obtained for this study, with waiver of informed consent for retrospective review of medical records. Dynamic susceptibility contrast-enhanced MR imaging data were obtained for 79 patients, and principal component analysis was applied to the perfusion signal intensity. The first six principal components were sufficient to characterize more than 99% of variance in the temporal dynamics of blood perfusion in all regions of interest. The principal components were subsequently used in conjunction with a support vector machine classifier to create a map of heterogeneity within the peritumoral region, and the variance of this map served as the heterogeneity score.

Results: The calculated principal components allowed near-perfect separability of tissue that was likely highly infiltrated with tumor and tissue that was unlikely infiltrated with tumor. The heterogeneity map created by using the principal components showed a clear relationship between voxels judged by the support vector machine to be highly infiltrated and subsequent recurrence. The results demonstrated a significant correlation ($r = 0.46$, $P < .0001$) between the heterogeneity score and patient survival. The hazard ratio was 2.23 (95% confidence interval: 1.4, 3.6; $P < .01$) between patients with high and low heterogeneity scores on the basis of the median heterogeneity score.

Conclusion: Analysis of dynamic susceptibility contrast-enhanced MR imaging data by using principal component analysis can help identify imaging variables that can be subsequently used to evaluate the peritumoral region in glioblastoma. These variables are potentially indicative of tumor infiltration and may become useful tools in guiding therapy, as well as individualized prognostication.

[1] From the Departments of Radiology (H.A., X.D., R.L.W., M.B., R.V., C.D.) and Neurosurgery (L.M., D.M.O.), University of Pennsylvania, 3600 Market St, Suite 380, Philadelphia, PA 19104. Received November 11, 2013; revision requested January 6, 2014; revision received March 5; accepted March 19; final version accepted April 29. **Address correspondence to** C.D. (e-mail: *Christos.Davatzikos@uphs.upenn.edu*).

Dynamic susceptibility contrast material–enhanced (DSC) magnetic resonance (MR) imaging is an important functional imaging method that enables quantitative assessment of tissue hemodynamic patterns. Aberration of blood flow, volume, and permeability is frequently observed during tumor growth, and characterization of these perfusion attributes has become clinically important for both diagnosis and therapy planning. In the context of glial neoplasms, perfusion characteristics have been shown to correlate with tumor type and grade (1) and hence influence treatment decisions. Glioblastoma is the most common and aggressive glial tumor in adults (2), with abnormal (tumor) tissue extending far beyond the visible, enhancing tissue on MR images (3). However, prevailing methods for perfusion data analysis yield little, if any, additional information in the surrounding peritumoral region. Furthermore, although measurements such as relative cerebral blood volume (rCBV), the most common method for analyzing and interpreting data obtained with DSC MR imaging, have shown promising correlations with both histologic grade and degree of neovascularization in gliomas (4,5), certain tissue characteristics and perfusion dynamics may not be fully captured by such global, one-dimensional variables (scalars).

DSC MR imaging is based on the principle that flow of a paramagnetic contrast agent through a capillary bed will transiently change the magnetic susceptibility of the given tissue (6). Decreased signal intensity on spin-echo or gradient-echo images after the first pass of the contrast agent, frequently described as susceptibility-induced T2* shortening, is the result of this temporal change in magnetic susceptibility. This signal time curve is then converted into a concentration time curve, and use of tracer kinetic analysis various hemodynamic variables, such as cerebral blood volume, cerebral blood flow, and mean transit time, as well as metrics that address vessel leakage, such as percentage signal recovery, may be estimated (7). Combined, these metrics enable microvascular imaging, providing a visual correlate of blood flow, volume, and vessel permeability (8,9).

However, calculation of these metrics is not only complicated but also involves various assumptions and model-dependent approximations (7). For example, bolus tracking relies on the assumption that the endothelial membrane is intact and there is no leakage of contrast agent, while fitting of a gamma-variate function to the concentration time curve is required to correct for tracer recirculation (10). Additionally, to calculate quantitative perfusion variables, the arterial input function, the concentration of contrast agent as a function of time, is frequently estimated from voxels near major arteries (7,10). Partly because of the postprocessing complexities involved with DSC MR imaging, commonly used variables in clinical use often describe the breadth of the perfusion signal, with only a couple of variables such as rCBV.

We hypothesized that additional, complementary features may be extracted from DSC MR images when the entire perfusion signal intenstiy is analyzed as a time series by using methods that capture all characteristics of the shape of this signal. The importance of the complete perfusion time series for tissue characterization has been highlighted previously. Chou et al demonstrated that noiseless independent factor analysis may be applied to DSC MR imaging data to extract spatiotemporal blood supply patterns in various tissue compartments (11). In turn, these patterns may be used to systematically classify tissue and improve the differentiation between normal and abnormal hemodynamics in a given tissue type.

In this work, we used dimensionality reduction methods to analyze the perfusion time series of patients with glioblastoma to identify tissue features that were not captured with currently calculated variables (eg, rCBV). To investigate the clinical utility of these multidimensional features, we used machine learning tools to analyze the heterogeneity of the peritumoral region. This region is an important tissue area in glioblastoma that leads to tumor recurrence in more

Advances in Knowledge

- Principal component analysis of perfusion time series, coupled with machine learning methods, offers a mathematically rigorous way of quantifying the full dynamics of blood perfusion in dynamic susceptibility contrast-enhanced MR imaging (>99%).
- These comprehensive measurements go beyond standard relative cerebral blood volume and may be used to extract peritumoral imaging features that highlight underlying subtle tissue heterogeneity ($P < .0001$).

Implications for Patient Care

- The method proposed in this article enables clinicians to visualize the heterogeneity of the peritumoral region in patients with glioblastoma and appreciate regions of subtly different imaging characteristics that would otherwise be missed visually.
- Imaging indexes derived with this approach seem to correlate with survival and recurrence and can therefore be used as predictive tools.

Published online before print
10.1148/radiol.14132458 **Content codes:** MR NR

Radiology 2014; 273:502–510

Abbreviations:
DSC = dynamic susceptibility contrast material–enhanced
rCBV = relative cerebral blood volume
ROI = region of interest
SVM = support vector machine

Author contributions:
Guarantors of integrity of entire study, H.A., L.M., X.D., D.M.O., C.D.; study concepts/study design or data acquisition or data analysis/interpretation, all authors; manuscript drafting or manuscript revision for important intellectual content, all authors; approval of final version of submitted manuscript, all authors; literature research, H.A., L.M., X.D., R.L.W., D.M.O.; clinical studies, H.A., X.D., R.L.W., D.M.O., C.D.; experimental studies, H.A., L.M., X.D., M.B., D.M.O., C.D.; statistical analysis, H.A., L.M., X.D., R.V., C.D.; and manuscript editing, all authors

Funding:
This research was supported by the National Institutes of Health (grant R01NS042645).

Conflicts of interest are listed at the end of this article.

than 80% of patients (12). The aim of this study was to augment the analysis of DSC MR imaging to uncover unique tissue characteristics that could potentially facilitate treatment planning through a better understanding of the peritumoral region in patients with glioblastoma.

Materials and Methods

Data Collection and Preprocessing

Institutional review board approval was obtained for this study, with waiver of informed consent for retrospective review of medical records. Patients treated at our institution for glioblastoma (World Health Organization grade IV) between July 2006 and December 2011 were retrospectively selected for our study. The inclusion criteria were patients with a sole tumor with preoperative advanced MR imaging (anatomic and perfusion imaging modalities). Subjects who had a prior tumor treated with radiation, surgery, or chemotherapy were excluded from the study. Nine patients were excluded because of multiple tumors, eight patients were excluded for missing perfusion MR imaging data, and six patients were excluded owing to prior resection. This resulted in 79 de novo patient samples, all of whom were treated with the same protocol. The clinical diagnosis of tumor recurrence was established via histopathologic report after repeat surgery to exclude pseudoprogression (13). All patients were imaged by using a 3-T MR imaging unit (Magnetom TrioTim; Siemens, Erlangen, Germany), and the image acquisition protocol was constant. With regard to the DSC sequence, the parameters were as follows: field of view, 22 cm; matrix, 128 × 128; pixel spacing, 1.72 × 1.72 mm; section thickness, 3 mm; and repetition time (msec)/echo time (msec), 45/2000. An initial loading dose of 3 mL of gadobenate dimeglumine (MultiHance; Bracco, Milan, Italy) was administered, which after 5 minutes was followed by another bolus injection with the remaining dose (for a total of 0.3 mL/kg or 1.5 times a single dose) during image acquisition.

For all MR imaging studies, the following preprocessing procedures were used (X.D., a medical image analyst with 6 years of experience). Smallest Univalue Segment Assimilating Nucleus, or SUSAN (14), a low-level image processing method, was used for noise reduction, and the nonparametric nonuniform intensity normalization, or N3 (15), algorithm was applied to correct for MR imaging intensity nonuniformity. Subsequently, image alignment was performed by using affine registration (the FMRIB [Functional MRI of the Brain] Linear Image Registration Tool, or FLIRT) (16), and skull stripping was performed by using the brain extraction tool (17) of the FMRIB Software Library, or FSL (18). Finally, Glioma Image Segmentation and Registration, or GLISTR (19), a technique that combines biophysical models of tumor growth with image-based tissue modeling, was used to create a segmentation mask of the enhancing tumor, as well as the peritumoral edematous tissue.

Calculation of Principal Components

Principal component analysis is a standard dimensionality reduction method (20) that was used to distill the 45-second DSC MR imaging time series down to a few variables (principal components) that capture the temporal dynamics of blood perfusion. In particular, the first principal component is a projection of the signal onto a direction that captures the highest amount of variance that can be captured by a single variable. Each succeeding component in turn has the highest variance possible under the constraint that it be uncorrelated with the preceding components. These components concurrently present various aspects of the shape of the perfusion time curve. The perfusion of each voxel was sampled at 45 time points, which were then used as the feature vector of the voxel in the principal components analysis, yielding 45 eigenvalues and, correspondingly, 45 components. We retained the number of components that accounted for more than 99% of the overall variance in the perfusion signal across individuals, indicating that the few principal components retained for further analysis captured almost all the perfusion dynamics present in the DSC MR imaging signal.

To characterize the perfusion characteristics of different brain tissues, several regions of interest (ROIs) were defined (white matter, gray matter, cerebrospinal fluid, edema, enhancing tumor, and nonenhancing tumor). Additionally, two ROIs were placed within the edema and/or peritumoral region, one immediately adjacent to the enhancing tumor (near) and the other at the distal edema boundary (far) (H.A. and L.M. by means of agreement; L.M. is a neurosurgery resident with 6 years of experience, and H.A. is an international medical graduate and medical imaging expert with 9 years of experience). The maximum width of these ROIs was two voxels to maintain region homogeneity and specifically did not include any area that was contrast enhancing. These two ROIs served as reference examples for near-tumor and far-from-tumor tissue, based on the expectation that they are likely to have relatively higher and lower infiltration, respectively (21,22), albeit they are merely modeling parameters and by no means imply anything about true underlying (unknown) infiltration.

The mean perfusion curve was computed for each ROI on the basis of the perfusion signal intensity time curve of all voxels in that ROI (Fig 1, left). Principal component analysis was subsequently used to capture the information of the perfusion time series in all ROIs and all subjects. The projections of data onto principal components contain the new coordinates of the data points. Because of the relative consistency in the perfusion pattern of the various ROIs, a feature vector consisting of the first six principal components was sufficient to capture more than 99% of the variance in the perfusion signal for all tissue types and all patients (Fig 1, right, depicts the first three components).

The conventional way to represent the perfusion signal is via delta R2*, which is calculated by dividing the signal to the value of the baseline and obtaining its logarithm to convert the signal into concentration time curves for single-echo data. Herein, however, our premise is to use machine learning methods to characterize the heterogeneity of the perfusion signal in edema, with the goal

Figure 1

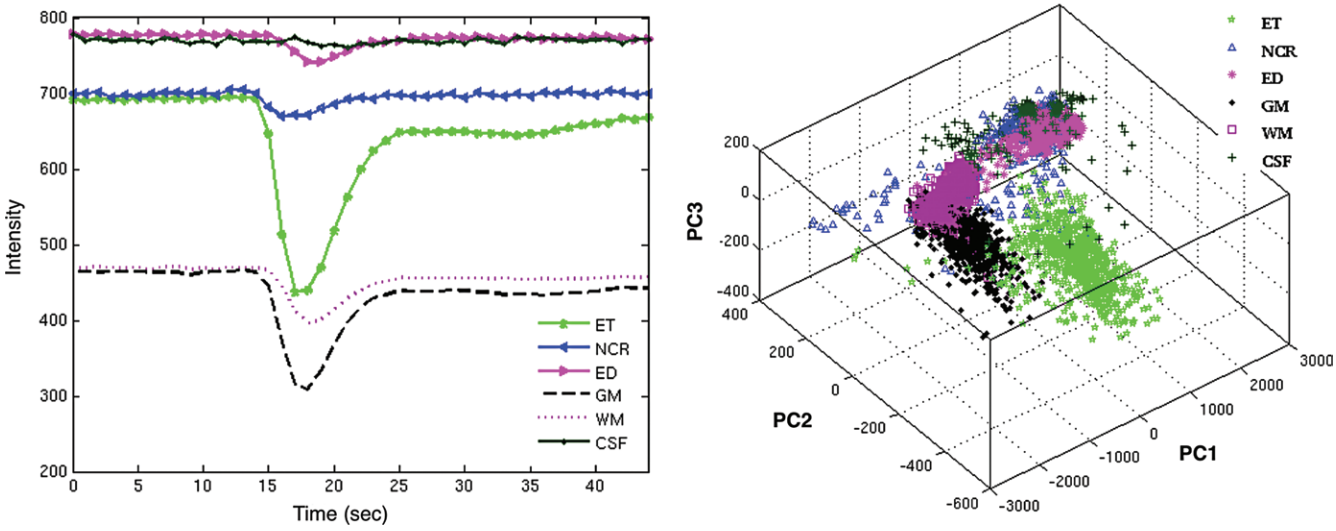

Figure 1: Graphs show perfusion time series and calculated principle components. Left: Graph shows the mean perfusion signal (DSC MR imaging time series) of all voxels for a given ROI. Right: The calculated principal components for each tissue type, based on the perfusion signal, are demonstrated. *CSF* = cerebrospinal fluid, *ED* = edema, *ET* = enhancing tumor, *GM* = gray matter, *NCR* = nonenhancing core, *PC1* = first principal component, *PC2* = second principal component, *PC3* = third principal component, *WM* = white matter.

Correlation Analysis

	Survival Analysis	
Variable	Correlation (*r* Value)	Significance (*P* Value)
Heterogeneity score	0.46	.00002
rCBV	0.04	.72
Delta R2*	0.35	.002

Note.—The correlation between perfusion imaging variables and survival is shown.

of predicting infiltration, recurrence, and survival. The transformations involved in calculating delta R2* might therefore not be optimal from this perspective and might remove (by removing baseline) or distort (by taking the logarithm) useful information from the perfusion signal. We therefore took the machine learning angle and used the raw MR signal, instead. However, the principal component analysis was applied to delta R2*, as well, to numerically prove the superiority of using raw data (Table).

Evaluation of Principal Components

The principal components incorporate different aspects of the dynamics of blood perfusion, including baseline signal, depth of signal decrease, slope of signal decrease and recovery, relative recovery, and so on (Fig 1, left). Hence, they capture and convey complex, high-dimensional information about a given tissue type as compared with the currently calculated scalars, such as rCBV. To investigate whether these principal components carried additional information, we focused our analysis on the peritumoral region. As noted previously, in this region, current perfusion measures fail to convey any useful information.

To accomplish this, we used support vector machines (SVMs) (23) to interpret the principal components of all voxels in the peritumoral region of a given patient. SVM is a learning model that analyzes data and recognizes patterns, which is used for classification. It takes a set of input data and predicts which of two possible classes forms the output. SVM was trained to create a classifier that, using the six principal components input features, aimed to distinguish between edematous peritumoral tissue immediately adjacent to the enhancing tumor and edematous tissue farther away. This schema was designed on the basis of the assumption that the former is likely to be relatively more highly infiltrated than the latter. In other words, based on the principal components of a given voxel, the SVM produced a score that was positive if the perfusion dynamics were similar to those in the low-infiltration ROI; in turn, a negative score was generated when the perfusion dynamics were similar to those of the high-infiltration ROI. This was performed on a voxel-by-voxel basis for the entire peritumoral region (H.A.).

The SVM was trained by using libSVM (24,25) with a Gaussian kernel function, and parameters were optimized on the basis of a cross-validated grid search. Subsequently, the SVM model was trained by using the projections of the near-far ROIs and

Figure 2

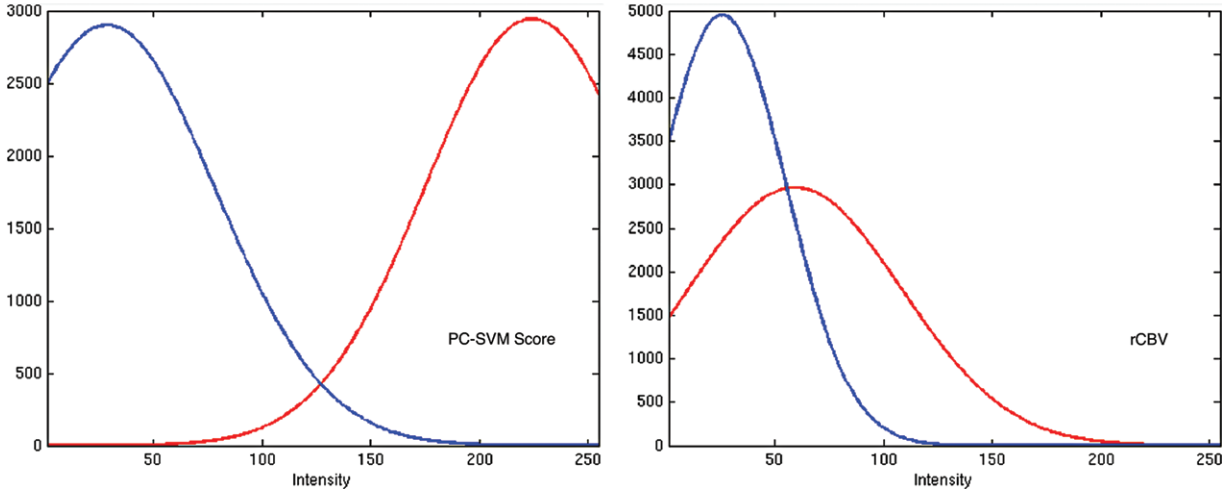

Figure 2: Graphs show separability of voxels within the peritumoral region. The figures demonstrate the separability of the near (likely infiltrated) and far (not infiltrated) ROIs within the peritumoral region. Red represents the probability density function of the near voxels, while blue represents the far voxels. Left: Graph, based on our method, shows two completely separable histograms (groups). Right: Graph, based on rCBV intensity values, shows overlapping histograms (the x-axis shows the intensity in arbitrary units scaled between 0 and 255, and the y-axis is the number of voxels).

applied to the rest of the peritumoral region. This process was repeated for all subjects, and the generated scores were used to produce a map of heterogeneity within the peritumoral region. The variance of these scores in the peritumoral region defined the heterogeneity score for a given test subject (H.A.). The heterogeneity score and the variance of rCBV within the peritumoral region were used to perform a correlation analysis between imaging variables and patient survival.

We evaluated the cluster heterogeneity to determine if this provided additional complementary information about a given tissue type beyond currently used scalar measures. For this analysis, we focused exclusively on the edematous peritumoral region. The SVM that was trained by using the high- and low-infiltration ROIs described earlier was applied to the entire peritumoral region. Resultant SVM scores were used to generate a "color scale" of heterogeneity within the peritumoral region.

In the absence of a correlate tissue sample from the disparate regions, we performed a qualitative comparison with postrecurrence MR imaging to assess what additional information these maps of heterogeneity carried. For this study, only patients who had no obvious residual tumor after initial resection based on data from all modalities, including rCBV, and had proven tumor recurrence at pathologic examination, were evaluated (by M.B., a neuroradiologist with 12 years of experience, with L.M. and H.A. by means of agreement).

All statistical analyses (correlation, hazard ratio, Kaplan-Meier curves) were performed by using a statistical software package (SPSS version 21; IBM, Armonk, NY) (X.D.). Correlation between imaging variables and survival was obtained by means of Pearson correlation. Subsequently, the subject group was dichotomized into high and low heterogeneity on the basis of the median heterogeneity score, and hazard ratios and Kaplan-Meier curves were computed for survival analysis, with the level of significance for a two-sided comparison set at 5% ($P < .05$).

Results

DSC MR Imaging Time Series

Five distinct periods were observed in the time series of DSC MR imaging image data, consistent with theoretical models and previous work (Fig 1) (10). Initial inspection of the perfusion time series in Figure 1 demonstrates that different brain tissues have unique perfusion dynamics. For example, the enhancing tumor region is, on average, associated with the largest signal decrease, while the peritumoral region has the smallest decrease in signal. The various ROIs also differ in their baseline signal intensity characteristics. Regions of edema and cerebrospinal fluid have the highest baseline signal intensity, while white and gray matter have the lowest. This is not unexpected, given that the DSC protocol is a T2*-weighted sequence.

Evaluation of Perfusion Time Series through Principal Components

When the perfusion time series are evaluated by using principal components, similar brain tissue forms characteristic clusters. These clusters, although heterogeneous, define a specific ROI (eg, nonenhancing tumor, Fig 1, right) and are separable from other tissues (clusters). More important, the calculated principal components of the high- and low-infiltration ROIs allow clear separability of these two important regions. Figure 2 illustrates the probability density function of the high- and low-infiltration ROIs, as calculated

Figure 3

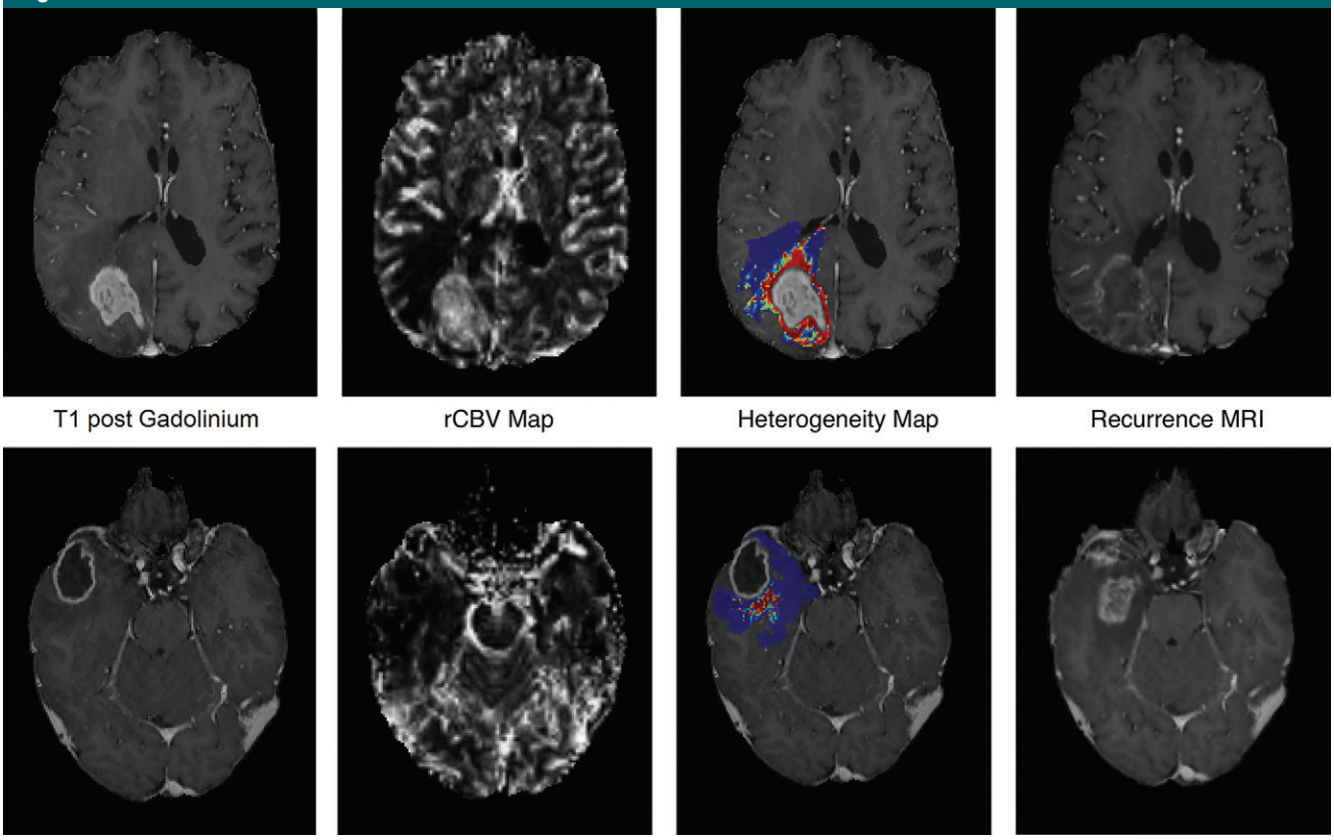

Figure 3: Maps of peritumoral heterogeneity demonstrate images obtained in two representative patients after principal components analysis. Left to right, the first column shows the preoperative T1-weighted gadolinium-enhanced image; the second column shows the rCBV map for each subject, in which the peritumoral region demonstrates relatively low, homogeneous perfusion. The third column shows the map of heterogeneity generated from the SVM scores within the peritumoral region. Red regions are areas most similar to highly infiltrated tissue, while blue regions are more similar to tissue with low infiltration. The last column depicts the T1-weighted gadolinium-enhanced image, at the same section, for each subject after tumor recurrence.

by using the described method (principal components SVM score), as well as the commonly computed perfusion measure (rCBV). While our method leads to two distinct, nonoverlapping histograms, the remaining perfusion measures do not afford the same level of tissue separability.

In Figure 3, this color scale map for two representative subjects is illustrated. Red areas depict regions that are most similar to the high-infiltration ROI, and blue depicts regions that are similar to the low-infiltration ROI. Images were registered by using affine registration (the FLIRT tool), as outlined in Materials and Methods. In most patients, the region of recurrence was in close proximity to the area judged by the SVM to be similar in perfusion characteristics to the high-infiltration ROI (Fig 3).

The results demonstrated a high and significant correlation ($r = 0.46$, $P < .0001$) between the heterogeneity of the peritumoral region and patient survival, while the score that used delta R2* had lower correlation ($r = 0.35$). On the contrary, the rCBV did not correlate with survival (Table). Figure 4 illustrates the Kaplan-Meier survival curves for high- and low-heterogeneity groups, respectively (hazard ratio, 2.23; 95% confidence interval: 1.4, 3.6; $P < .01$). Finally, support vector regression analysis demonstrated that the first six principal components captured the information conveyed by the common perfusion measure, rCBV ($r = 0.94$).

Figure 5 provides a visual representation of the first four principal components extracted from the DSC MR imaging perfusion data. In Figure 5 (plots), the first four principal eigenvectors obtained from all voxels are plotted after being multiplied by ±2 standard deviations of the respective principal components. These plots indicate that the different principal components were found to relate to different aspects of the perfusion curves: *(a)* Principal component 1 was found to primarily relate to the global baseline signal level at each voxel; *(b)* principal component 2 has the greatest variability around the baseline and the depth

Figure 4

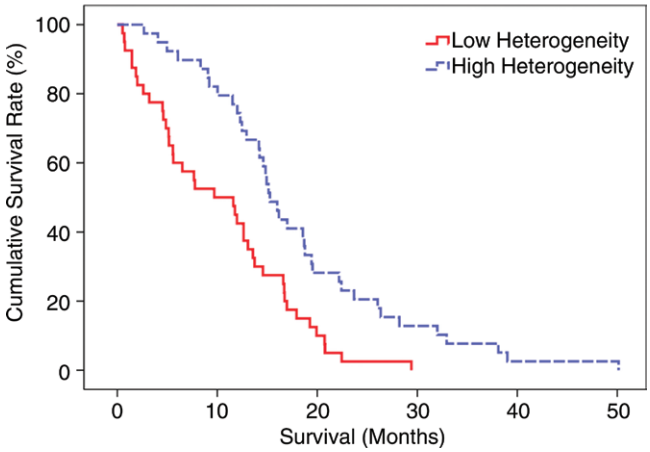

Figure 4: Graph shows the Kaplan-Meier survival curve for the three subject groups, with low (red), medium (orange), and high (green) heterogeneity, respectively. The analysis was based on 79 subjects that were dichotomized according to the heterogeneity score. The calculated hazard ratio for the low-heterogeneity group is 2.23 (95% confidence interval: 1.4, 3.6; $P < .01$).

of the curve; therefore, it conveys the depth of the signal decrease in relation to the baseline level; *(c)* principal component 3 reflects more complex information—namely, the shape of the perfusion signal—in other words, how steep the signal decrease and recovery are; and *(d)* principal component 4 appears to be driven by the baseline signal and its recovery.

Discussion

The proposed method highlights the heterogeneity of the peritumoral region by using the temporal dynamics of DSC MR imaging. This heterogeneity map, which is constructed by using advanced but easy-to-implement analytical techniques, demonstrates the clinical relevance of this region. Notably, we found that the heterogeneity within this region is significantly and robustly correlated with patient survival and

Figure 5

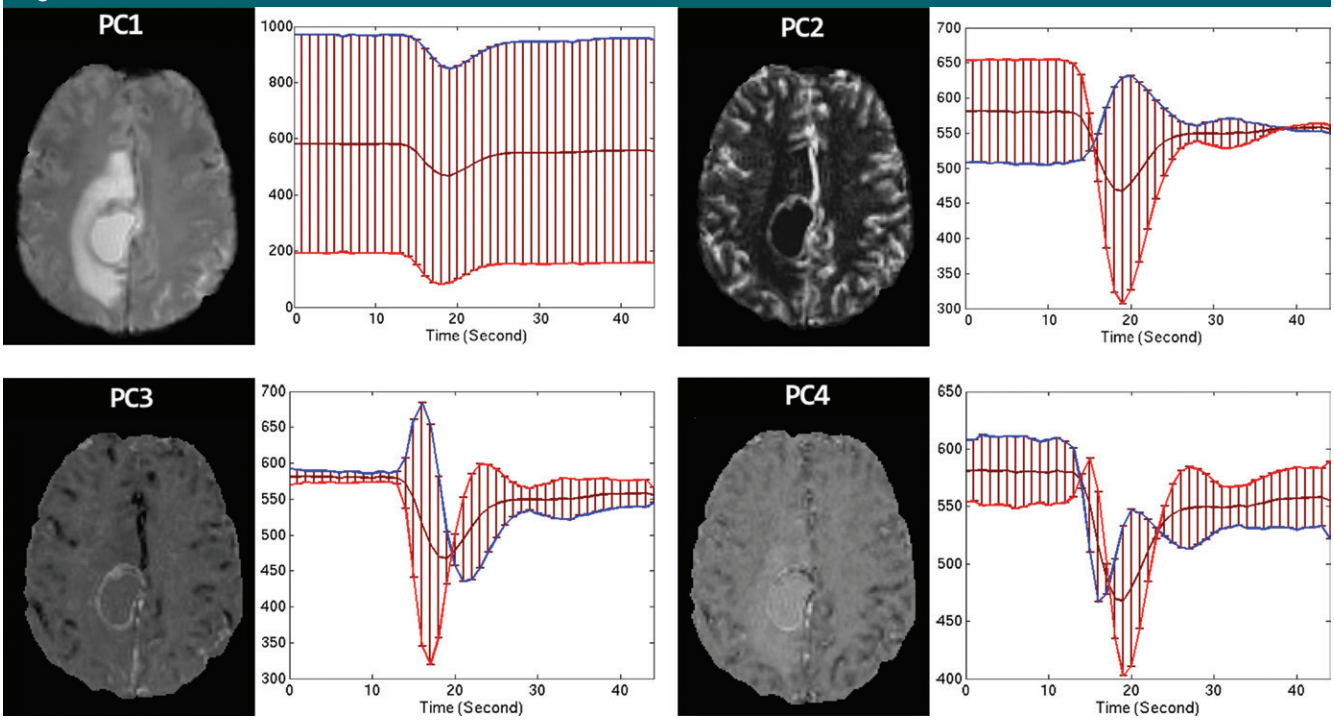

Figure 5: Principal component images and plots demonstrate the first four principal components of an MR image (left), along with the plot of the corresponding principal eigenvector (right), shown to illustrate the breadth of information contained within the perfusion time-series. The plots have been constructed from the perfusion signal of all voxels, with the error bar representing ±2 standard deviations of the respective principal component. Red and blue lines represent the negative and positive parts of principal components, respectively. *PC1* = first principal component, *PC2* = second principal component, *PC3* = third principal component, *PC4* = fourth principal component.

offers insight into potential future tumor recurrence. This information is completely obscured when the perfusion signal is analyzed in the traditional manner. Thus, this method not only highlights the importance of the peritumoral region in glioblastoma but also shows how information from this region, when analyzed in this manner, can bring to light important clinical information that may otherwise have been missed.

The peritumoral region remains a critical problem in both the understanding and treatment of glioblastoma. Although it has been shown previously (3,26) that edema results from infiltrating tumor cells, edema also occurs as a biological response to the angiogenic and vascular permeability factors released by the spatially adjacent tumor cells (27). With the proposed method, information that is extracted is currently obscured when analyzing perfusion images by using prevailing techniques, and our preliminary results demonstrate that this information (tissue heterogeneity) may reflect tumor invasion, as evidenced by the close spatial relationship with tumor recurrence. These results are strengthened by the fact that our approach does not require any assumptions or approximations, and, more important, are clinically relevant as substantiated by the strong correlation between our calculated heterogeneity score and patient survival. Thus, although DSC MR imaging without a correlate pathologic specimen cannot demonstrate the heterogeneity of the peritumoral region, our calculated heterogeneity score can be used to differentially classify this important tissue region.

A limitation of this study is lack of a biological reference index, such as histopathologic correlation with surgical specimens from the peritumoral infiltrated areas that would be addressed in a future study. Another limitation of our approach relates to the specialized nature of principal component analysis and SVM and the lack of availability of related software on regular clinical workstations. However, both principal component analysis and SVM are widely understood and described procedures, with lots of free software available for their application. Moreover, our own software pipeline is freely available for use.

In summary, advanced imaging techniques are increasingly used in the clinical evaluation of human gliomas. DSC MR imaging has already been applied to differentiate glioblastoma from brain metastasis, predict glioma grade, and distinguish recurrence from radiation necrosis (26). In the present study, informative features were extracted from the temporal dynamics of DSC MR imaging by using principal component analysis, and these variables were used via SVM classification to highlight the heterogeneity of the peritumoral region. Although preliminary, this method may help identify highly malignant regions that would have otherwise not been recognized by using current techniques. The results of this study represent the methods for analyzing the MR perfusion signal that enable improved characterization of the peritumoral region, as well as localization of highly infiltrated areas. In turn, this information may be used to augment targeted therapy and provide patient-specific prognostication.

Disclosures of Conflicts of Interest: H.A. disclosed no relevant relationships. **L.M.** disclosed no relevant relationships. **X.D.** disclosed no relevant relationships. **R.L.W.** disclosed no relevant relationships. **M.B.** disclosed no relevant relationships. **R.V.** disclosed no relevant relationships. **D.M.O.** Activities related to the present article: author received a diagnostic imaging grant from Celldex Therapeutics. Activities not related to the present article: author has a patent broadly related to the work. Other relationships: disclosed no relevant relationships. **C.D.** disclosed no relevant relationships.

References

1. Thompson G, Mills SJ, Coope DJ, O'Connor JP, Jackson A. Imaging biomarkers of angiogenesis and the microvascular environment in cerebral tumours. Br J Radiol 2011; 84(Spec No 2):S127–S144.
2. Yang I, Aghi MK. New advances that enable identification of glioblastoma recurrence. Nat Rev Clin Oncol 2009;6(11):648–657.
3. Konukoglu E, Clatz O, Bondiau PY, Delingette H, Ayache N. Extrapolating glioma invasion margin in brain magnetic resonance images: suggesting new irradiation margins. Med Image Anal 2010;14(2):111–125.
4. Tykocinski ES, Grant RA, Kapoor GS, et al. Use of magnetic perfusion-weighted imaging to determine epidermal growth factor receptor variant III expression in glioblastoma. Neuro-oncol 2012;14(5):613–623.
5. Aronen HJ, Gazit IE, Louis DN, et al. Cerebral blood volume maps of gliomas: comparison with tumor grade and histologic findings. Radiology 1994;191(1):41–51.
6. Rosen BR, Belliveau JW, Vevea JM, Brady TJ. Perfusion imaging with NMR contrast agents. Magn Reson Med 1990;14(2):249–265.
7. Østergaard L. Principles of cerebral perfusion imaging by bolus tracking. J Magn Reson Imaging 2005;22(6):710–717.
8. Wolf RL, Detre JA. Clinical neuroimaging using arterial spin-labeled perfusion magnetic resonance imaging. Neurotherapeutics 2007;4(3):346–359.
9. Covarrubias DJ, Rosen BR, Lev MH. Dynamic magnetic resonance perfusion imaging of brain tumors. Oncologist 2004;9(5): 528–537.
10. Barbier EL, Lamalle L, Décorps M. Methodology of brain perfusion imaging. J Magn Reson Imaging 2001;13(4):496–520.
11. Chou YC, Teng MM, Guo WY, Hsieh JC, Wu YT. Classification of hemodynamics from dynamic-susceptibility-contrast magnetic resonance (DSC-MR) brain images using noiseless independent factor analysis. Med Image Anal 2007;11(3):242–253.
12. Hochberg FH, Pruitt A. Assumptions in the radiotherapy of glioblastoma. Neurology 1980; 30(9):907–911.
13. Barajas RF Jr, Chang JS, Segal MR, et al. Differentiation of recurrent glioblastoma multiforme from radiation necrosis after external beam radiation therapy with dynamic susceptibility-weighted contrast-enhanced perfusion MR imaging. Radiology 2009;253(2): 486–496.
14. Smith SM, Brady JM. SUSAN—a new approach to low level image processing. Int J Comput Vis 1997;23(1):45–78.
15. Sled JG, Zijdenbos AP, Evans AC. A nonparametric method for automatic correction of intensity nonuniformity in MRI data. IEEE Trans Med Imaging 1998;17(1):87–97.

16. Jenkinson M, Smith S. A global optimisation method for robust affine registration of brain images. Med Image Anal 2001;5(2):143–156.

17. Smith SM. Fast robust automated brain extraction. Hum Brain Mapp 2002;17(3):143–155.

18. Jenkinson M, Beckmann CF, Behrens TE, Woolrich MW, Smith SM. FSL. NeuroImage 2012;62(2):782–790.

19. Gooya A, Pohl KM, Bilello M, et al. GLISTR: glioma image segmentation and registration. IEEE Trans Med Imaging 2012;31(10):1941–1954.

20. Pearson K. LIII. On lines and planes of closest fit to systems of points in space. Philos Mag Ser 6 1901;2(11):559–572.

21. Yamahara T, Numa Y, Oishi T, et al. Morphological and flow cytometric analysis of cell infiltration in glioblastoma: a comparison of autopsy brain and neuroimaging. Brain Tumor Pathol 2010;27(2):81–87.

22. Guo J, Yao C, Chen H, et al. The relationship between Cho/NAA and glioma metabolism: implementation for margin delineation of cerebral gliomas. Acta Neurochir (Wien) 2012;154(8):1361–1370; discussion 1370.

23. Cortes C, Vapnik V. Support-vector networks. Mach Learn 1995;20(3):273–297.

24. Chang CC, Lin CJ. LIBSVM: a library for support vector machines. ACM Trans Intell Syst Technol 2011;2(3):27.

25. Drucker H, Burges CJ, Kaufman L, Smola A, Vapnik V. Support vector regression machines. In: Advances in neural information processing systems 9. Cambridge, Mass: MIT Press, 1997; 155–161.

26. Barajas RF Jr, Phillips JJ, Parvataneni R, et al. Regional variation in histopathologic features of tumor specimens from treatment-naive glioblastoma correlates with anatomic and physiologic MR Imaging. Neuro-oncol 2012;14(7):942–954.

27. Chang EL, Akyurek S, Avalos T, et al. Evaluation of peritumoral edema in the delineation of radiotherapy clinical target volumes for glioblastoma. Int J Radiat Oncol Biol Phys 2007;68(1):144–150.